al Kimiya: Jurnal Ilmu Kimia dan Terapan
p-ISSN: 2407-1897, e-ISSN: 2407-1927
Vol. 10, No. 1 (57-63), Juni 2023/Dzulhijah 1444

EFFECT OF LOW SOLID/LIQUID RATIO ON HYDROTHERMAL SYNTHESIS OF HYDROXYAPATITE WITH GREEN TEMPLATE FROM BANANA FLOWER (*Musa acuminata Cavendish*)

FERLI SEPTI IRWANSYAH[1,2*], ALFI IKHLASUL AMAL[3], EKO PRABOWO HADISANTOSO[3], ATIEK ROSTIKA NOVIYANTI[2], DIANA RAKHMAWATY EDDY[2], AZMAN BIN MA'AMOR[4], AND RISDIANA[5]

[1]Department of Chemistry Education, Faculty of Tarbiyah and Teacher Training, UIN Sunan Gunung Djati, Bandung, Indonesia

[2]Department of Chemistry, Faculty of Mathematics and Natural Sciences, Universitas Padjadjaran, Sumedang, Indonesia

[3]Department of Chemistry, Faculty of Science and Technology, UIN Sunan Gunung Djati, Bandung, Indonesia

[4]Department of Chemistry, Universiti Malaya, Kuala Lumpur, Malaysia

[5]Department of Physics, Faculty of Mathematics and Natural Sciences, Universitas Padjadjaran, Sumedang, Indonesia

*Corresponding author email: ferli@uinsgd.ac.id

Article Information

Received: Mar 27, 2023
Revised: Jun 14, 2023
Accepted: Jun 23, 2023
Published: Jun 30, 2023

DOI: 10.15575/ak.v10i1.25262

Keywords:
Hydroxyapatite; hydrothermal; solid/liquid ratio; green template; banana flower.

Abstract

Hydroxyapatite (HA) was successfully synthesized using the hydrothermal method. This study aimed to analyze the effect of a low solid/liquid ratio on the properties of HA crystals. HA synthesis was performed using chicken eggshells and the hydrothermal method at a temperature of 150°C. The solvent amount was kept constant, while the solid amount varied (half-reaction). The characteristics of HA were determined using XRD, FTIR, PSA, and SEM. The results showed that the purity and size of HA were influenced by a low solid/liquid ratio, while the crystallinity remained relatively unchanged, directly impacting the lattice parameter value. FTIR analysis revealed the absence of the O-H group in the sample with the low solid/liquid ratio. PSA results showed a smaller particle size of 0.995 µm for the sample with the low solid/liquid ratio. SEM results demonstrated a smaller particle size in the sample with a low solid/liquid ratio when observed at the same magnification.

INTRODUCTION

Hydroxyapatite (HA) is one of the most widely studied biomaterials in the medical field due to its proven biocompatibility and its role as the main component of the mineral composition of bones and teeth. HA also serves as an important source of calcium and phosphate, which are required for remineralization of demineralized areas of enamel [1]. Due to its unique properties, such as its ability to chemically bond with bone [2], its non-toxic and non-inflammatory nature [3], and its direct stimulation of bone growth through osteoblast activation [4], HA is synthesized using various methods. Multiple techniques have been developed for HA synthesis, including precipitation [5], sol-gel [6], biomimetic deposition [7], electrophoresis [8], and hydrothermal synthesis [9].

Hydrothermal synthesis involves the use of an autoclave vessel and reactor to subject an aqueous precursor to high-pressure, high-temperature conditions [10]. Hydrothermal techniques are widely employed for the preparation of various inorganic compounds, including HA. Physicists, chemists, materials scientists, engineers, and many others commonly utilize this technique. The hydrothermal method is highly valued for its ability to control morphological characteristics and ensure product purity, which sets it apart from conventional methods [11] [12].

In many studies involving the hydrothermal synthesis method, discussions often revolve around the correlation between raw material composition, initial treatment, synthesis conditions, post-reaction treatment, and the resulting phase or material phase. However, there is a limited number of studies that explore the apparent relationship and

combination of solid and liquid ratios, especially for HA materials. In a previous study, Wałek (2008), it was observed that a low solid/liquid (S/L) ratio led to a significant increase in fly ash dissolution (up to 85 wt%) within the first 4 hours of the reaction. It was demonstrated that, under the commonly employed S/L ratios (50–150 g/dm^3), fly ash dissolution was largely restricted, resulting in the formation of zeolite crystals on the surface of partially dissolved fly ash particles [13]. In this paper, we aim to reduce the uncertainty by utilizing a low solid/liquid ratio during the synthesis process, with a specific focus on HA materials.

Furthermore, this paper discusses the utilization of egg shells as a calcium source, employing a green template derived from banana flower parts. The synthesized materials were subsequently characterized using X-Ray Diffraction (XRD), Fourier Transform Infrared Spectroscopy (FTIR), Particle Size Analyzer (PSA), and Scanning Electron Microscopy (SEM).

EXPERIMENT

Material

The materials used in this research include $(NH_4)_2HPO_4$ (pa Sygma Aldrich), NH_4OH (pa Sygma Aldrich), deionized water, and filter paper, chicken eggshells as calcium precursors for the synthesis of hydroxyapatite, banana flowers extracted from the heart of a banana plant, and aquadest.

Instrumentation

Instrumentation utilized in this research comprises XRD (PANalytical-X'Pert HighScore), SEM (JEOL JCM 6000), FTIR (Thermo Scientific BDM1910155), and PSA (Particle Size Analyzer) of the Horiba SZ 100 model.

Procedure

This research procedure was divided into four stages: the eggshell calcination stage; the template extraction stage from banana plant parts; the NHA synthesis stage with the green template from banana plant parts; and the NHA characterization stage.

Eggshell Calcination

To convert $CaCO_3$ in eggshells into CaO, a calcination process was conducted. First, the chicken eggshells were washed with clean water, then ground using a mortar and pestle, and sieved through a 120-mesh sieve. The sieved particles were then calcined at 1000°C for 5 hours to obtain calcium oxide powder.

Template Extraction from Banana Flower

For template extraction, the flower parts were initially washed with distilled water and rinsed with acetone. Next, they were cut into small pieces, with the banana flower separated from the male bud. The cut parts were then stored in an oven at 60°C for 24. The oven-dried parts were ground to a smooth consistency and further boiled. A total of 20 g of the milled product was boiled in 250 mL of water for 10 minutes, followed by filtration to obtain filtrate.

NHA Synthesis with Templates from Banana Flower

For the synthesis of NHA 150, 2.8648 g of calcium oxide powder was placed into a 100 mL autoclave, and 5 mL of banana flower extract with an 8% concentration was added. The mixture was stirred until smooth. Then, 3.9501 g $(NH_4)_2HPO_4$ was added dropwise while stirring slowly, adding ammonia solution to maintain pH 10.

For the synthesis of ½ NHA 150, 1.4324-gram calcium oxide powder was put into a 100 mL autoclave, added as much as 5 mL of extract of the banana flower with concentrations of 8%, then stirred until smooth. Then 1.9750 grams of $(NH_4)_2HPO_4$ was added dropwise while stirring slowly, and ammonia solution to maintain pH 10 was added to maintain a pH of 10.

Each mixture was heated at 150°C for 24 hours, filtered, and the filtrate was collected. The solid phase of the synthesized NHA filtrate was washed with deionized water, then dried at 100°C for 24 hours. The dried material was ground with mortal and pestle and sieved to obtain particles of uniform size.

In the sample code, the numbers 1 and ½ represent the solid/liquid ratio. The number 1 is used to denote the normal solid/liquid ratio for comparison purposes. Meanwhile, ½ indicates a low solid/liquid ratio, where the amount of solids used is half of the normal ratio while maintaining the same amount of liquid. The code "NHA" stands for nano-hydroxyapatite, while 150 represents the synthesis temperature employed (NHA 150 and ½ NHA 150).

RESULT AND DISCUSSION

Calcination of Chicken Eggshells

In the calcination process, $CaCO_3$ decomposes into CaO from 750°C until completely decomposes when the temperature is 1000°C. The reactions that occur are [14] [15]:

$$CaCO_3(s) \xrightarrow[\Delta]{1000°C} CaO(s) + CO_2(g) \quad (1)$$

Figure 1 compares egg shells before and after the calcination process. Loss of Ignition (Lol) due to the decomposition of chicken eggshells from $CaCO_3$ to CaO is 64.32%. The resulting CaO is then used as a calcium precursor in the NHA formation reaction with $(NH_4)_2HPO_4$ as a phosphate precursor and banana flower parts as a template following the reaction (2). Flower extract on banana plant parts is used because it is easy to obtain and contains as much as 3.97% pectin [16] and other phytochemicals that can help control morphology and reduce the size of nanoparticle crystals.

$$10CaO_{(s)} + 6(NH_4)_2HPO_{4\ (s)} + 4H_2O_{(aq)} \rightarrow Ca_{10}(PO_4)_6(OH)_{2\ (s)} + 20NH_4OH_{(aq)} \quad (2)$$

Figure 1. Egg shells A) before and B) after the calcination process.

XRD Characterization of NHA

The XRD NHA 150 data were compared with the XRD ½ NHA 150 data. The analysis results can be seen in **Figure 2** and **Table 1**. From the X-ray diffraction pattern data, the crystallographic characteristics of the crystals can be determined. The typical HA peaks on the diffractograms of the three synthesized HA samples appear at 2θ = 25°, 31°, and 32°. The peaks correspond to the peaks on HA from ICSD: 01-089-6440. In addition, it is known that the crystal structure of HA obtained from all synthesis conditions is hexagonal with a P 63/m space group. However, apart from the typical peaks of HA, other peaks indicate the presence of an impurity phase at 2θ ~ 17.9°. These peaks show a typical peak for portlandite ($Ca(OH)_2$) [17] [18].

The degree of crystallinity is determined by comparing the crystalline area fraction with the sum of the crystalline area fraction and the amorphous area fraction which can be calculated from XRD data using the Debye-Scherrer equation, equation (3) below [15]:

$$Xc = 100 \times \frac{(I_{300} - V_{112/300})}{I_{300}} \quad (3)$$

where I300 is the intensity of the diffraction peak at (300), V112/300 is the intensity of (112) and (300). The purity of NHA 150 is 93%, with impurities in the $Ca(OH)_2$ phase of 7%. While ½ NHA 150 has a purity of 94% with impurities in $Ca(OH)_2$ of 6%. The difference in purity is influenced by the half-reaction system with excess solvent for the synthesis of HA in the hydrothermal method. The crystallinity percentage of HA ½ NHA 150 is 80.39%, and the percentage value of crystallinity obtained is relatively the same compared to NHA 150 (crystallinity = 79.14%). These findings prove that a low solid/liquid ratio affects the crystallinity of the HA obtained, although not much [19].

Table 1. The crystallite size and percentage of crystallinity of NHA 150 and ½ NHA 150.

Samples	XRD	
	Crystallite size	Crystallinity
NHA 150	26.05 nm	79.14 %
½ NHA 150	23.22 nm	80.39 %

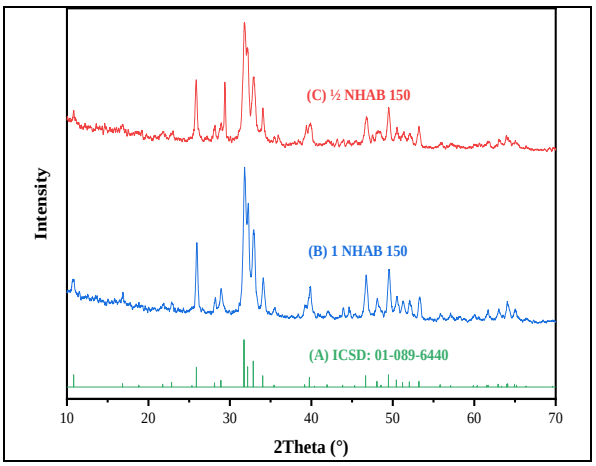

Figure 2. Comparison of peak intensity database (A) ICSD: 01-089-6440 with (B) NHA 150 and (C) ½ NHA 150.

The crystal size of NHA 150 is 26.05 nm, while ½ NHA 150 has a crystal size of 23.22 nm. By looking at the data generated, we can say that the crystals formed belong to the nanocrystals. The difference in crystal size obtained from the results of this synthesis could indicate that a low solid/liquid ratio can affect the crystal size of HA. Crystal size decreased monotonically with increasing and was associated with increasing crystal nucleation rate, thus achieving high solute concentration (supersaturation) [18]. In hydrothermal synthesis, product formation and stability are affected by reaction conditions such as reagent concentration, temperature, pressure, and pH [20] [21].

FTIR Characterization of NHA

The FTIR characterization aims to identify the functional groups present in the NHA sample. Each peak in the absorbance band was compared with the literature. FTIR results can be seen in **Figure 3** and **Table 2**.

The spectrum's characteristic peaks represent each sample's chemical composition within the wavenumber range of 400–4000 cm^{-1}. For both NHA samples, the transmittance bands in the wavenumber range 1022, 560, and 600 cm^{-1} correspond to the asymmetric triply degenerate stretching and bending vibration of phosphate (PO_4^{3-}) ion associated with HA lattice respectively. The 1450 cm^{-1} band reveals small incorporation of CO_3^{2-} in HA structure due to environmental CO_2. The peak at 630 cm−1 and the wide peak at 3560–3700 cm−1 indicate the stretching vibrations of OH^- ion HA crystals which prove the presence of an HA phase [22] [23].

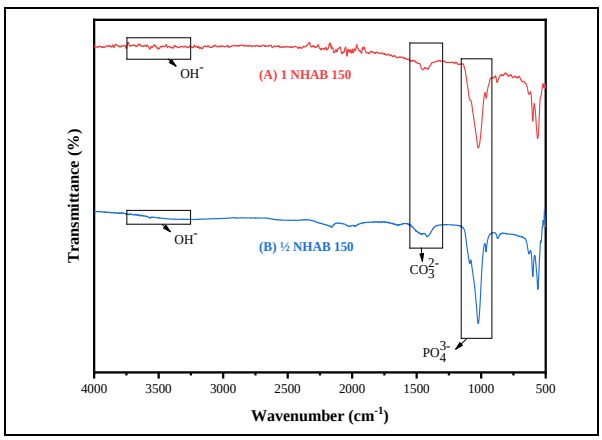

Figure 3. FTIR spectrum of (A) NHA 150 and (B) ½ NHA 150.

In sample NHA 150, water absorption bands were detected (3700-2500 and at 1630 cm^{-1}). In the ½ NHA 150 sample, each absorption band at 3700-2500 cm^{-1} is very small and the band at 1630 cm^{-1} is absent. It seems that the amount of water as a reaction medium affects the area of collisions between substances. In the ½ NHA 150 sample, the amount of water is more so that the formation and association of crystallites occur more quickly. When the settling process is slow, fewer water molecules are trapped in the inclusions. Further, an increase in the drying temperature used to dry the crystals causes a loss of the absorption band at 3400 cm^{-1} [24] [25].

Table 2. Bands (in cm^{-1}) identified in the FTIR spectra for NHA 150 and NHA 150.

Bond type	NHA 150	½ NHA 150
PO_4^{3-} stretching	562.32 960.75	560.90 961.65
PO_4^{3-} asymmetric stretching	1022.13	1022.79
PO_4^{3-} asymmetric bending	600.11	500.56
Free O–H stretching	3567.69	3566.51
O–H bending	630.41	630.60
CO_3^{2-}	1414.98	1417.99

PSA Characterization of NHA

Figure 4 and **Table 3** show the particle size of the synthesized NHA. **Figure 4a** results from particle size analysis for NHAB 150, where the particle distribution is 0.580-1.967µm. **Figure 4b** results from particle size analysis for NHAB 150, where the particle distribution is 0.740-1.741µm. Based on these results, it is known that the particle distribution of each NHA sample is generally uniform [26]. With a more uniform size, the suspended particles will be stable due to a lower size deviation. If the particle size deviation is high, the particles will more easily experience agglomeration faster. The wide particle size distribution will lead to low suspension stability. The low PI value indicates that stabilizers can prevent agglomeration between particles [27] [28]. When compared to the crystal size, the particle size value will always be bigger than the crystal size. This is because the particles are composed of crystals.

Table 3. The particle size of synthesized NHA.

Sample	Particle Size (µm)	Polydispersity Index (PI)
NHAB 150	1.305	0.989
½ NHAB 150	0.995	1.304

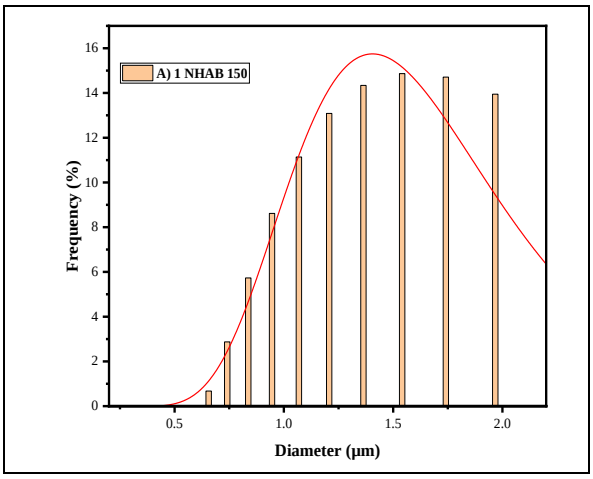

(A)

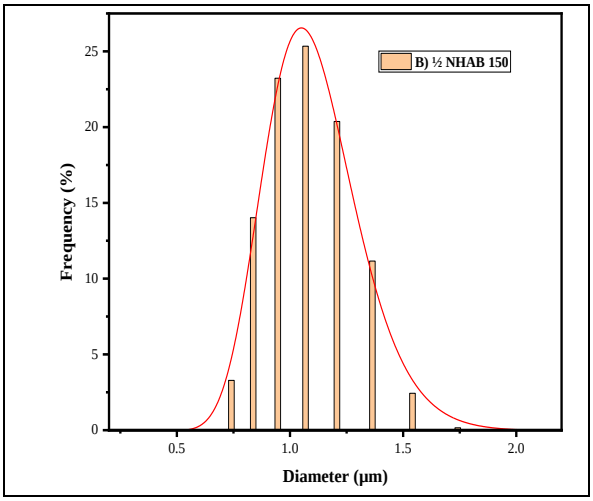

(B)

Figure 4. Particle distribution of the synthesized (A) NHA 150 and (B) ½ NHA 150.

SEM Characterization of NHA

The morphology for each NHA is shown in **Figure 5**. The morphology of each NHA is shown in Figure 5. From both of them, it can be seen that the morphology formed is spherical with a hexagonal shape. **Figure 5A** is the morphology for NHA 150, in this section also visible NHA particles overlap with other particles. **Figure 5B** is the morphology for ½ NHA 150, it can be seen that in this section the morphological catchment area is larger than **Figure 5A** even though each test was carried out at the same magnification, namely at 3,500 x. This shows that the particle size for ½ NHA 150 is smaller than NHA 150, this is following the PSA results which show that ½ NHA 150 has a smaller particle size. Differences in the shape of NHA particles will affect the body's biological response, cytotoxicity, the size of NHA, and the adaptation of bone cells to NHA itself [29].

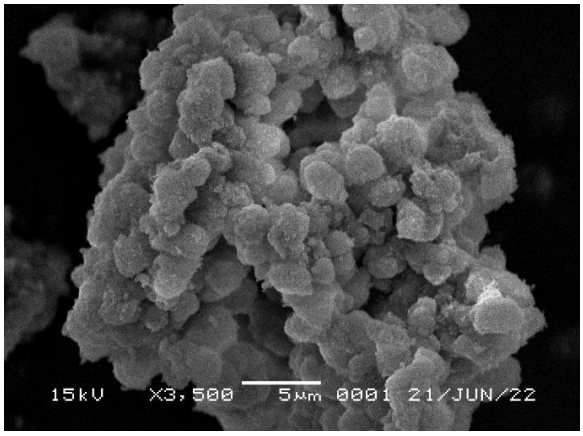

(A)

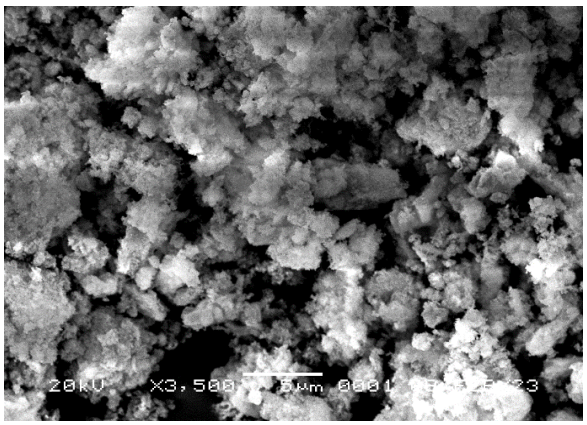

(B)

Figure 5. SEM image of (A) NHA 150 and (B) ½ NHA 150.

CONCLUSION

This research successfully synthesized HA using the hydrothermal method. All experimental results show that a low solid/liquid ratio has an impact on the characteristics of HA. The results demonstrate that the low solid/liquid ratio affects both the purity and size of HA, while the crystallinity remains relatively consistent, directly influencing the lattice value parameters. The FTIR results reveal the absence of O-H groups in samples with a low solid/liquid ratio. PSA results indicate that samples with a low solid/liquid ratio possess smaller particle sizes of 0.995 µm. SEM results demonstrate that the structure of the samples with a low solid/liquid ratio exhibits smaller particle sizes at the same magnification.

ACKNOWLEDGEMENT

The authors thank LITAPDIMAS, DIKTIS for funding this research work and the facilities from Universitas Padjadjaran, Indonesia, by Academic Leadership Grant (ALG).

REFERENCES

[1] E. Pepla, L.K. Besherat, G. Palaia, G. Tenore, and G. Migliau, "Nano-hydroxyapatite and its applications in preventive, restorative and regenerative dentistry: a review of literature", *Ann Stomatol (Roma)*, **5**(3), 108-114, 2014.

[2] F.B. Bagambisa, U. Joos, and W. Schilli, "Mechanisms and structure of the bond between bone and hydroxyapatite ceramics", *Journal of Biomedical Materials Research*, **27**(8), 1047-1055, 1993, doi: 10.1002/jbm.820270810.

[3] X. Zhao, S. Ng, B.C. Heng, J. Guo, L. Ma *et al.*, "Cytotoxicity of hydroxyapatite nanoparticles is shape and cell-dependent", *Archives of Toxicology*, **87**(6), 1037-1052, 2013, doi: 10.1007/s00204-012-0827-1.

[4] A. Bassi, J. Gough, M.Zakikhani, and S.Downes, "Bone tissue regeneration", *Electrospinning for Tissue Regeneration*, Sawston, Woodhead Publishing, 93-110, 2011, doi: 10.1533/9780857092915.2.93.

[5] M. Kalpana and R. Nagalakshmi, "Effect of reaction temperature and pH on structural and morphological properties of hydroxyapatite from precipitation method", *Journal of the Indian Chemical Society*, **100**, (4), 100947, 2023, doi: 10.1016/j.jics.2023.100947.

[6] O.A. Osuchukwu, A. Salihi, I. Abdullahi, P.O. Etinosa, and D.O. Obada, "A comparative study of the mechanical properties of sol-gel derived hydroxyapatite produced from a novel mixture of two natural biowastes for biomedical applications", *Materials Chemistry and Physics*, **297**, 127434, 2023, doi: 10.1016/j.matchemphys.2023.127434.

[7] B. Čolović, V. Jokanović, B. Jokanović, and N. Jovic, "Biomimetic deposition of hydroxyapatite on the surface of silica thin film covered steel tape", *Ceramics International*, **40**(5), 6949-6955, 2014, doi: 10.1016/j.ceramint.2013.12.018.

[8] C. Su, Y. Su, Z. Li, M.A. Haq, Y. Zhou, and D. Wang, "In situ synthesis of bilayered gradient poly(vinyl alcohol)/hydroxyapatite composite hydrogel by directional freezing-thawing and electrophoresis method", *Materials Science and Engineering: C*, **77**, 76-83, 2017.

[9] H.O. LeClerc, G.A. Tompsett, A.D. Paulsen, A.M. McKenna, S.F. Niles *et al.*, "Hydroxyapatite catalyzed hydrothermal liquefaction transforms food waste from an environmental liability to renewable fuel", *iScience*, **25**(9), 104916, 2022, doi: 10.1016/j.isci.2022.104916.

[10] V. Vendruscolo, D.L. Fritzen dan E.A. de Mattos, and L.C.V. Rodrigues, "Light storage perovskites: Synthesis, mechanisms, and applications", in *Perovskite Ceramics*, Amsterdam, Elsevier, 517-546, 2023, doi: 10.1016/B978-0-323-90586-2.00013-9.

[11] P. Kumar, M.C. Mathpal, G.K. Inwati, H.C. Swart, and W.D. Roos, "Graphene oxide-based semiconducting nanomaterial's composites for environmental applications", in *Nanoscale Compound Semiconductors and their Optoelectronics Applications*, Sawston, Woodhead Publishing, 407-431, 2022, doi: 10.1016/B978-0-12-824062-5.00002-6.

[12] W.l. Xu, B. Liu, Y.C. Wang, G.Y. Xiao, X. Chen *et al.*, "A facile strategy for one-step hydrothermal preparation of porous hydroxyapatite microspheres with core–shell structure", *Journal of Materials Research and Technology*, **17**, 320-328, 2022. https://doi.org/10.1016/j.jmrt.2022.01.001.

[13] T.T. Wałek, F. Saito, and Q. Zhang, "The effect of low solid/liquid ratio on hydrothermal synthesis of zeolites from fly ash", *Fuel*, **87**(15-16), pp. 3194-3199, 2008, doi: 10.1016/j.fuel.2008.06.006.

[14] A.R. Toibah, F. Misran, A. Shaaban, and Z. Mustafa, "Effect of pH condition during hydrothermal synthesis on the properties of hydroxyapatite from eggshell waste", *Journal of Mechanical Engineering and Sciences*, **13**(2), 4958-4969, 2019, doi: 10.15282/jmes.13.2.2019.14.0411.

[15] V.R. Lugo, E.S. Rodriguez, R.A Vazquez, K. Aleman, and A.L. Rivera, "Hydroxyapatite synthesis from a starfish and β-tricalcium phosphate using a hydrothermal method", *Royal Society of Chemistry*, **7**, 7631-7639, 2017, doi: 10.1039/C6RA26907A.

[16] Y.A. Begum and S.C. Deka, "Chemical profiling and functional properties of dietary fiber rich inner and outer bracts of culinary banana flower", *Journal of Food Science and Technology*, **56**(12), 5298–5308, 2019.

[17] A.R. Noviyanti, N. Akbar, Y. Deawati, E.E. Ernawati, Y.T. Malik, R.P. Fauzia, and Risdiana, "A novel hydrothermal synthesis of nanohydroxyapatite from eggshell-calcium-oxide precursors", *Heliyon*, 6(4), e03655, 2020, doi: 10.1016/j.heliyon.2020.e03655.

[18] K.W. Goh, Y.H. Wong, S. Ramesh, H. Chandran, S. Krishnasamy, S. Ramesh, A. Sidhu, and W. Teng, "Effect of pH on the properties of eggshell-derived hydroxyapatite bioceramic synthesized by wet chemical method assisted by microwave irradiation", *Ceramics International*, **47**(7), 8879-8887, 2021, doi: 10.1016/j.ceramint.2020.12.009.

[19] M. Baladi, M. Amiri, P. Mohammadi, K.S. Mahdi, Z. Golshani *et al*., "Green sol–gel synthesis of hydroxyapatite nanoparticles using lemon extract as capping agent and investigation of its anticancer activity against human cancer cell lines (T98, and SHSY5)", *Arabian Journal of Chemistry*, **16**(4), 104646, 2023, doi: 10.1016/j.arabjc.2023.104646.

[20] S.H. Daryan, A. Khavandi, and J. Javadpour, "Surface engineered hollow hydroxyapatite microspheres: Hydrothermal synthesis and growth mechanisms", *Solid State Sciences*, **106**, 106301, 2020, doi: 10.1016/j.solidstatesciences.2020.106301.

[21] N.K.V. Nadimpalli, R. Bandyopadhyaya, and V. Runkana, "Thermodynamic analysis of hydrothermal synthesis of nanoparticles," *Fluid Phase Equilibria"*, **456**, 33-45, 2017, doi: 10.1016/j.fluid.2017.10.002.

[22] T. Chatterjee, M. Ghosh, M. Maji, M. Ghosh, S. K. Pradhan dan A. K. Meikap, "Study of microstructural and electrical properties of silver substituted hydroxyapatite for drug delivery applications", *Materials Today Communications*, **31**, 103360, 2022, doi: 10.1016/j.mtcomm.2022.103360.

[23] B.P. Kafle, "Infrared (IR) spectroscopy", in *Chemical Analysis and Material Characterization by Spectrophotometry*, Nepal, Elsevier, 2020, doi: 10.1016/B978-0-12-814866-2.00007-5.

[24] S. Koutsopoulos, "Synthesis and characterization of hydroxyapatite crystals: A review study on the analytical methods", *Journal of Biomedical Materials Research*, **62**(4), 600-612, 2022, doi: 10.1002/jbm.10280.

[25] J. Tao, "FTIR and raman studies of structure and bonding in mineral and organic–mineral composites", in *Methods in Enzymology*, Washington, Elsevier, 2013, doi: 10.1016/B978-0-12-416617-2.00022-9.

[26] S.R. Yenti, A. Fadli, Wisrayetti, A. Amri, D. Novandri *et al*., "Synthesis of hydroxyapatite powder using natural latex particles as", *Materials Today: Proceedings*, **79**, 2023, doi: 10.1016/j.matpr.2023.03.282.

[27] V.K. Yadav, K.K. Yadav, G. Gnanamoorthy, N. Choudhary, S.H. Khan *et al*., "A novel synthesis and characterization of polyhedral shaped amorphous iron oxide nanoparticles from incense sticks ash waste", *Environmental Technology & Innovation*, **20**, 101089, 2020, doi: 10.1016/j.eti.2020.101089.

[28] I. Nugrahani and W.N. Auli, "Diclofenac-proline nano-co-crystal development, characterization, in vitro dissolution and diffusion study", *Heliyon*, **6**(9), e04864, 2020, doi: 10.1016/j.heliyon.2020.e04864.

[29] X. Zhao, S. Ng, B.C. Heng, J. Guo, L. Ma *et al*., "Cytotoxicity of hydroxyapatite nanoparticles is shape and cell dependent," *Archives of Toxicology*, **87**(6), 1037-1052, 2013, doi: 10.1007/s00204-012-0827-1.

[30] J.S. Earl, D.J. Wood, and S. J. Milne, "Hydrothermal synthesis of hydroxyapatite", *Journal of Physics: Conference Series*, **26**, 268–271, 2006.